Nonlinear Growth of a Line-tied g-Mode Near Marginal Stability

P. Zhu, C. C. Hegna, and C. R. Sovinec
University of Wisconsin-Madison
Center for Plasma Theory and Computation
Madison, WI 53706

Abstract

A theoretical framework has been developed for the study of the nonlinear gravitational (g-) mode of a line-tied flux tube near marginal stability. The theory is based on an expansion using two small parameters, $\epsilon \sim |\boldsymbol{\xi}|/L_{\rm eq} \ll 1$, and $n^{-1} \sim k_{\|}/k_{\perp} \ll 1$, with $\boldsymbol{\xi}$ denoting the plasma displacement, $L_{\rm eq}$ the characteristic equilibrium scale, $k_{\|}$ and $k_{\perp}$ the dominant wavenumber of perturbation parallel and perpendicular to equilibrium magnetic field lines respectively. When $\epsilon \sim n^{-1}$, the Cowley-Artun regime is recovered where plasma is to the lowest order incompressible [S. C. Cowley and M. Artun, Phys. Rep., **283**, 185-211 (1997)]. The detonation regime where the nonlinear growth of the mode is finite-time singular is a narrower subset of the Cowley-Artun regime. However, the validity of this regime breaks down when $\epsilon \gg n^{-1}$. In the intermediate nonlinear phase when $\epsilon \sim n^{-1/2}$, the lowest order plasma compression [$\sim \nabla \cdot \boldsymbol{\xi} \sim \mathcal{O}(1)$] is nonzero. Direct MHD simulations with both a finite difference code and NIMROD indicate that the mode remains bounded in magnitude with a slightly reduced nonlinear growth [P. Zhu, A. Bhattacharjee, and K. Germaschewski, to appear in PRL (2006); P. Zhu, C. C. Hegna, and C. R. Sovinec, DPP2005]. During this phase, the coupled growth of the mode amplitude $\boldsymbol{\xi}$ and plasma compression may contribute to a nonlinear stabilization. The corresponding governing model equations for this intermediate nonlinear phase are derived.

I. INTRODUCTION

Nonlinear ballooning instability has received growing interests during recent years. In modern tokamak experiments, high-β regimes with very large plasma pressure gradient in both internal and external transport barrier regions have been routinely achieved in various high-performance confinement states. The degradation and termination of the high-confinement states, characterized with the disruption of transport barriers in high-β regimes, are often the outcome of the excitation and nonlinear development of MHD instabilities, such as ballooning instability. In the case of external transport barrier, the periodic collapse of edge pedestal of a H-mode plasma, a phenomenon known as the Edge Localized Mode (ELM), has close associations with the onset of peeling-ballooning instabilities in the pedestal region [1, 2]. The largest ELM events (type-I) can lead to large thermal energy and particle losses and have the potential to seriously damage tokamak wall and divertors. This is particularly the concern for H-mode operational regimes of ITER, which are characterized with the high-β and high fraction of bootstrap current driven by large pressure gradient in the edge. It is therefore crucial to understand and predict the growth and saturation of the nonlinear MHD (peeling-ballooning) instabilities associated with ELMs.

Nonlinear ballooning instability is also a candidate mechanism for a class of large scale, fast disruptions in space plasmas, including the substorm onset in the Earth's magnetotail [3–5] and solar coronal mass ejections (CME) [6, 7]. Traditional scenarios mostly invoke magnetic reconnection as the underlying process. Reconnection scenarios explain many features of the observations. One major drawback of the reconnection model for the fast disruptions of flux tubes in space plasma, however, is that they still have difficulty explaining the fast time scale observed in those events [8]. Because of the two-dimensional (2D) nature of the reconnection models usually used in those studies, flute-like ballooning modes with small wavelength traveling perpendicular to the 2D plane of reconnection are generally missing in those models. It is speculated that ballooning instabilities should introduce additional and major disruptions in the high-β regime, which is exactly the regime of space plasma in the near-Earth plasma sheet (6-15 R_E) [9] and in middle to upper corona (10-100 Mm) [10], which are the sites of substorm onset and CME, respectively. In addition, there is emerging evidence that disruptions in space plasmas are not always the direct outcome of magnetic reconnections. For example, in the near-Earth magnetotail, substorm events

have been observed to take place prior to the occurrence and away from the site of magnetic reconnections in the middle magnetotail [11]. In all those events, nonlinear ballooning instability may provide the secondary or primary mechanism needed to fully explain the disruption process.

Like magnetic reconnection, nonlinear ballooning instability is a universal process in magnetized plasma. However, unlike magnetic reconnection, nonlinear ballooning instability is a subject less studied or understood, mainly due to three reasons. First, until recent years, fusion plasmas are mostly in very low β regimes; space plasmas engaging in reconnection process, such as those in solar corona, have traditionally been considered as force-free. Advances in both fusion experiment and space observation have brought new interests in the instabilities of high-β plasmas. Second, ballooning mode, particularly in high-β plasmas, involves the interaction of kinetic, magnetic, and internal energy of the plasma. This adds a level of complication not present in the kinetic-magnetic interaction characterizing kink mode and magnetic reconnection process in a low β regime. Third, ballooning instability is a multi-scale process that combines a global structure along, a meso structure across, and a local structure perpendicular to field lines. The multiple scales involved bring considerable complexity and difficulty, such as anisotropy and stiffness, to the nonlinear analysis of the mode, in both theory and simulations.

A geometrically simpler variant of ballooning instability is the gravitational or g- mode of a line-tied flux tube. For the g-mode, the equilibrium magnetic field lines can be straight, and gravity plays an equivalent role to the magnetic field line curvature for ballooning instability. Because of the simpler geometry, the nonlinear dynamics of g-mode appears to be more amenable to analysis. For this reason, we focus on the study of the nonlinear g-mode as the first step towards the understanding of the nonlinear ballooning instability in more sophisticated geometries.

Earlier, Cowley and Artun [12] developed an MHD model for the nonlinear g-mode of line-tied flux tubes near marginal stability. Their model admits a detonation regime where the nonlinear g-mode develops finite-time singularity, exhibiting fast-than-exponential ("explosive") growth. The theory was later extended to model the nonlinear ballooning instabilities in Earth's magnetotail [13] and in tokamak plasma [14]. The detonation regime of the nonlinear ballooning instability models has been invoked to explain the current sheet disruption during a substorm onset and the rapid edge plasma pedestal loss during ELMs.

Such a regime, however, has not been observed in direct ideal MHD simulations of nonlinear g-mode [15, 16] or in direct resistive MHD simulations of nonlinear ballooning instability [17–20].

In this work, we have developed a theoretical framework for the study of a generic nonlinear ballooning instability. It has been applied to the nonlinear gravitational (g-) mode of a line-tied flux tube in particular. At the order $\epsilon = n^{-1}$, the Cowley-Artun regime [12] is recovered where the plasma is to the lowest order incompressible. The detonation regime where the nonlinear growth of the mode is finite-time singular is a narrower subset of the Cowley-Artun regime. In the intermediate nonlinear phase when $\epsilon = n^{-1/2}$, the lowest order plasma compression [$\nabla\cdot\boldsymbol{\xi} \sim \mathcal{O}(1)$] is nonzero and direct MHD simulations indicate that the mode continue to grow exponentially [16]. The governing model equations for this nonlinear phase have been derived.

We lay out our theory framework in Sec. II. The linear and nonlinear g-mode structures are described in III and IV respectively. The highlight of this paper is given in Sec. IV B, where our nonlinear analysis is supported by direct MHD simulation results, and the governing model equations for the intermediate nonlinear phase are presented. Finally, summary and discussions are presented in Sec. V.

II. THEORY FRAMEWORK

A Lagrangian formulation of the ideal MHD equations is used for our analysis [12, 21]. In particular, the equation of motion can be written as

$$\frac{\rho_0}{J}\nabla_0\mathbf{R}\cdot\frac{\partial^2\boldsymbol{\xi}}{\partial t^2} = -\nabla_0\left[\frac{p_0}{J^\gamma}+\frac{\left(\mathbf{B}_0\cdot\nabla_0\mathbf{R}\right)^2}{2J^2}\right]+\nabla_0\cdot\left[\frac{\mathbf{B}_0}{J}\cdot\nabla_0\left(\frac{\mathbf{B}_0}{J}\cdot\nabla_0\mathbf{R}\right)\right]+\frac{\rho_0}{J}\nabla_0\mathbf{R}\cdot\mathbf{g} \quad (1)$$

where

$$\mathbf{R}(\mathbf{r}_0,t)=\mathbf{r}_0+\boldsymbol{\xi}(\mathbf{r}_0,t),\quad \nabla_0=\frac{\partial}{\partial\mathbf{r}_0},\quad J(\mathbf{r}_0,t)=|\nabla_0\mathbf{R}|$$

To analyze Eq.(1), two small parameters

$$\epsilon\sim\frac{|\boldsymbol{\xi}|}{L_{\rm eq}}\ll 1,\qquad n^{-1}\sim\frac{k_\parallel}{k_\perp}\sim\frac{L_y}{L_z}\ll 1 \quad (2)$$

and a nonlinear ballooning expansion of the form

$$\boldsymbol{\xi}(\sqrt{n}x_0,ny_0,z_0,t)=\sum_{i=1}^{\infty}\sum_{j=0}^{\infty}\epsilon^i n^{-\frac{j}{2}}\left(\hat{x}\xi_{x\{i,j\}}+\frac{\hat{y}}{\sqrt{n}}\xi_{y\{i,j\}}+\hat{z}\xi_{z\{i,j\}}\right) \quad (3)$$

are introduced. The MHD equation in (1) is expanded accordingly. Here, we define the perturbation spatial scales $x = \sqrt{n}x_0$, $y = ny_0$, $z = z_0$; $L_{\rm eq}$ denotes the characteristic equilibrium scale; L_y and L_z are domain sizes in y and z directions, and $k_\parallel$ and $k_\perp$ the dominant wavenumber of perturbation parallel and perpendicular to equilibrium magnetic field lines respectively. The relative magnitudes of the three components of the displacement vector are chosen in accordance with conventional linear theory on ballooning modes. Recent direct simulations have indicated that such an ordering still holds in the early to intermediate nonlinear phases of the g-mode evolution [16].

III. LINEAR STRUCTURE (1ST ORDER IN ϵ)

We write Eq. (1) as

$$I_\alpha(\boldsymbol{\xi}) = F_\alpha(\boldsymbol{\xi}) \qquad (\alpha = x, y, z)$$

where $I_\alpha(\boldsymbol{\xi})$ denotes the inertial term on the left hand side, and $F_\alpha(\boldsymbol{\xi})$ denotes the force term on the right hand side. Specifically they are expanded as follows

$$I_\alpha(\boldsymbol{\xi}) = \sum_{i=0}^{\infty}\sum_{j=-3}^{\infty} \epsilon^i n^{-\frac{j}{2}} I_{\alpha\{i,j\}}, \qquad F_\alpha(\boldsymbol{\xi}) = \sum_{i=0}^{3}\sum_{j=-3}^{6} \epsilon^i n^{-\frac{j}{2}} F_{\alpha\{i,j\}}$$

At the zeroth order of ϵ, the equation simply represents the force balance of the equilibrium

$$0 = F_{x\{0,0\}} = -p' - \frac{(B^2)'}{2} - \rho g, \quad \text{where} \quad (\cdot)' \equiv \frac{d}{dx_0}(\cdot) \tag{4}$$

Within the first order expansion in ϵ, the expansion of Eq. (1) in $n^{-\frac{1}{2}}$ reveals the ballooning structure of the linear g-mode. The first few leading order expansions in $n^{-\frac{1}{2}}$ are listed here.

$$I_{x\{1,j\}} = \rho\partial_t^2 \xi_{x\{1,j\}}, \qquad j = 0, 1, 2, \cdots \tag{5}$$

$$F_{x\{1,-2\}} = (B^2 + \gamma p)\partial_x J_{\{1,-1\}} \tag{6}$$

$$\begin{aligned} F_{x\{1,-1\}} &= \left[\rho g + (B^2)' + \gamma p'\right] J_{\{1,-1\}} \\ &\quad + (B^2 + \gamma p)\partial_x J_{\{1,0\}} - \rho g \partial_x \xi_{x\{1,0\}} - B^2 \partial_{xz}^2 \xi_{z\{1,0\}} \end{aligned} \tag{7}$$

$$\begin{aligned} F_{x\{1,j\}} &= \left[\rho g + (B^2)' + \gamma p'\right] J_{\{1,j\}} - (B^2)'\partial_z \xi_{z\{1,j\}} + B^2 \partial_z^2 \xi_{x\{1,j\}} \\ &\quad + (B^2 + \gamma p)\partial_x J_{\{1,j+1\}} - \rho g \partial_x \xi_{x\{1,j+1\}} - B^2 \partial_{xz}^2 \xi_{z\{1,j+1\}}, \\ &\quad j = 0, 1, 2, \cdots \end{aligned} \tag{8}$$

$$I_{y\{1,j\}} = \rho\partial_t^2 \xi_{y\{1,j-1\}}, \qquad j = 1, 2, 3, \cdots \tag{9}$$

$$F_{y\{1,-3\}} = (B^2+\gamma p)\partial_y J_{\{1,-1\}} \tag{10}$$

$$F_{y\{1,j\}} = (B^2+\gamma p)\partial_y J_{\{1,j+2\}} - \rho g\partial_y \xi_{x\{1,j+2\}} - B^2\partial_{yz}^2 \xi_{z\{1,j+2\}}, \quad j=-2,-1,0, \tag{11}$$

$$F_{y\{1,j\}} = B^2\partial_z^2 \xi_{y\{1,j-1\}} + (B^2+\gamma p)\partial_y J_{\{1,j+2\}} - \rho g\partial_y \xi_{x\{1,j+2\}} - B^2\partial_{yz}^2 \xi_{z\{1,j+2\}}, \quad j=1,2,3,\cdots \tag{12}$$

$$I_{z\{1,j\}} = \rho\partial_t^2 \xi_{z\{1,j\}}, \qquad j=0,1,2,\cdots \tag{13}$$

$$F_{z\{1,-1\}} = \gamma p\partial_z J_{\{1,-1\}} \tag{14}$$

$$F_{z\{1,j\}} = \gamma p\partial_z J_{\{1,j\}} - \rho g\partial_z \xi_{x\{1,j\}}, \qquad j=0,1,2,\cdots \tag{15}$$

Here $J_{\{i,j\}}$ is the coefficient of $\epsilon^i n^{-\frac{j}{2}}$ in the expansion of Jacobian $J(\mathbf{r}_0,t)$, and

$$J_{\{1,-1\}} = \partial_x \xi_{x\{1,0\}} + \partial_y \xi_{y\{1,0\}} \tag{16}$$

$$J_{\{1,j\}} = \partial_z \xi_{z\{1,j\}} + \partial_x \xi_{x\{1,j+1\}} + \partial_y \xi_{y\{1,j+1\}}, \qquad j=0,1,2,\cdots \tag{17}$$

A. Linear Ballooning-g Mode: Growth Equation

With an eikonal approximation $\boldsymbol{\xi} \sim \exp(-k_y y)$, where $k_y \sim n^{-1}$, we obtain the local eigenmode equations (aligned along each field line at a given x_0) from above expansions:

$$\partial_t^2 \xi_{x\{1,0\}} = \frac{B^2}{\rho}\partial_z^2 \xi_{x\{1,0\}} + \frac{g[(\gamma-2)p' - \rho g]}{B^2(1+\gamma\beta)}\xi_{x\{1,0\}} + \frac{(1+2\beta)\gamma p' + (1+2\gamma\beta)\rho g}{\rho(1+\gamma\beta)}\partial_z \xi_{z\{1,0\}} \tag{18}$$

$$\partial_t^2 \xi_{z\{1,0\}} = \frac{\gamma p}{\rho(1+\gamma\beta)}\partial_z^2 \xi_{z\{1,0\}} - \frac{g}{1+\gamma\beta}\partial_z \xi_{x\{1,0\}} \tag{19}$$

The two coupled eigenmode equations strongly resemble those for a linear ballooning mode in a curved magnetic field [22, 23]. It is worth noting that linear ballooning-like eigenmodes always involve plasma and magnetic compressions. Only near marginal stability when $\tau_A^2\partial_t^2 \ll 1$ (where $\tau_A \equiv \sqrt{\rho}/B$ denoting the time that it takes a local shear Alfvén wave traveling over a unit distance along field lines), compressions may be negligible and reduced to zero for local modes along open, free end field lines. However, for closed field lines, and for field lines with line-tied boundary condition, plasma compression may not be reducible even near marginal stability. In those cases, the coupled eigenmode equations in

(18) and (19) reduce to a single differential-integral eigenmode equation

$$\frac{B^2}{\rho}\partial_z^2\xi_{x\{1,0\}} + g\left[\left(\frac{p'}{p}+\frac{\rho g}{\gamma p}\right)\xi_{x\{1,0\}} - \left(\frac{\beta'}{\beta}+\frac{\rho g}{\gamma p}\right)\frac{\left\langle\xi_{x\{1,0\}}\right\rangle}{1+\gamma\beta}\right] = \Gamma^2\xi_{x\{1,0\}} \simeq 0, \tag{20}$$

where

$$\left\langle\xi_{x\{1,0\}}\right\rangle \equiv \frac{1}{L_z}\int_0^{L_z} dz\xi_{x\{1,0\}},$$

over the domain $0 < z < L_z$ and $\Gamma(x_0)$ is the local eigenvalue (growth rate) along each field line.

B. Linear Ballooning-g Mode: Envelope Equation

The local eigenmode equation $\mathcal{L}H(z) = \Gamma^2 H(z)$ only determines the mode structure $H(z)$ along field lines. The global mode can take the form

$$\xi_{x\{1,0\}} = \xi_{x(1)}(x,y,\tau)H(z), \quad (\tau = n^{-\frac{1}{2}}t) \tag{21}$$

assuming $\Gamma^2/\Gamma_{\rm A}^2 \sim \mathcal{O}(n^{-1})$ near marginal stability, where $\Gamma_{\rm A}^2 \equiv B^2/\rho = \tau_A^{-2}$. At next two orders of $n^{-\frac{1}{2}}$

$$\mathcal{L}\xi_{x\{1,1\}} = \Gamma^2\xi_{x\{1,1\}} \simeq 0, \tag{22}$$

$$\Gamma^2\partial_y^2\xi_{x\{1,0\}} = \partial_y^2\mathcal{L}\xi_{x\{1,2\}} + \frac{B^2}{\rho}\partial_z^2\partial_x^2\xi_{x\{1,0\}}, \tag{23}$$

where

$$J_{\{1,-1\}} = \partial_x\xi_{x\{1,0\}} + \partial_y\xi_{y\{1,0\}} = 0, \tag{24}$$

has been used. Using

$$\left\langle H(z)\mathcal{L}\xi_{x\{1,2\}}\right\rangle \sim \mathcal{O}(n^{-1})\xi_{x\{1,2\}} \sim 0, \tag{25}$$

together with line-tying boundary condition in x and no-slip boundary condition in z (which is equivalent to perfect conducting wall boundary condition in both x and z directions), we recover the envelope equation with the Connor-Hastie-Taylor ballooning structure [24]

$$\frac{\langle H^2\rangle}{\Gamma_{\rm A}^2}\partial_y^2\partial_\tau^2\xi_{x(1)} = \frac{\Gamma^2}{\Gamma_{\rm A}^2}\left\langle H^2\right\rangle\partial_y^2\xi_{x(1)} + \left\langle (H')^2\right\rangle\partial_x^2\xi_{x(1)}, \tag{26}$$

where $H \equiv dH/dz$.

IV. NONLINEAR STRUCTURE (2ND AND HIGHER ORDER IN ϵ)

From the second and higher order expansions in ϵ, we obtain the nonlinear structure of the g-mode. Due to the limit of space, we list only the second order expansion below. Here the notion $A^{(i,j,k)} \equiv \frac{\partial}{\partial x^i}\frac{\partial}{\partial y^j}\frac{\partial}{\partial z^k}A$ is used.

$$F_{x\{2,-3\}} = (B^2+\gamma p)J^{(1,0,0)}_{\{2,-2\}} - \left[3B^2+\gamma(\gamma+1)p\right]J_{\{1,-1\}}J^{(1,0,0)}_{\{1,-1\}} \tag{27}$$

$$\begin{aligned}
F_{x\{2,-2\}} &= \left[\rho g + (B^2)' + \gamma p'\right]J_{\{2,-2\}} + (B^2+\gamma p)J^{(1,0,0)}_{\{2,-1\}} \\
&\quad - \left[2\rho g + 3(B^2)' + \gamma(\gamma+1)p'\right]\frac{J^2_{\{1,-1\}}}{2} \\
&\quad - \left[3B^2+\gamma(\gamma+1)p\right](J_{\{1,0\}}J^{(1,0,0)}_{\{1,-1\}} + J^{(1,0,0)}_{\{1,0\}}J_{\{1,-1\}}) \\
&\quad + B^2(2J^{(1,0,0)}_{\{1,-1\}}\xi^{(0,0,1)}_{z\{1,0\}} + 2J_{\{1,-1\}}\xi^{(1,0,1)}_{z\{1,0\}} - J^{(0,0,1)}_{\{1,-1\}}\xi^{(1,0,0)}_{z\{1,0\}}) \\
&\quad + \rho g J_{\{1,-1\}}\xi^{(1,0,0)}_{x\{1,0\}}
\end{aligned} \tag{28}$$

$$\begin{aligned}
F_{x\{2,-1\}} &= \left[\rho g + (B^2)' + \gamma p'\right]J_{\{2,-1\}} \\
&\quad + (B^2+\gamma p)J^{(1,0,0)}_{\{2,0\}} - \rho g\xi^{(1,0,0)}_{x\{2,0\}} - B^2\xi^{(1,0,1)}_{z\{2,0\}} \\
&\quad - \left[2\rho g + 3(B^2)' + \gamma(\gamma+1)p'\right]J_{\{1,-1\}}J_{\{1,0\}} \\
&\quad - \left[3B^2+\gamma(\gamma+1)p\right]\left(J_{\{1,1\}}J^{(1,0,0)}_{\{1,-1\}} + J_{\{1,0\}}J^{(1,0,0)}_{\{1,0\}} + J_{\{1,-1\}}J^{(1,0,0)}_{\{1,1\}}\right) \\
&\quad + 2(B^2)'J_{\{1,-1\}}\left(\xi_z\right)^{(0,0,1)}_{\{1,0\}} \\
&\quad - B^2\left(2J_{\{1,-1\}}\left(\xi_x\right)^{(0,0,2)}_{\{1,0\}} + J^{(0,0,1)}_{\{1,-1\}}\left(\xi_x\right)^{(0,0,1)}_{\{1,0\}}\right) \\
&\quad + B^2\left(2J^{(1,0,0)}_{\{1,0\}}\left(\xi_z\right)^{(0,0,1)}_{\{1,0\}} + 2J_{\{1,0\}}\left(\xi_z\right)^{(1,0,1)}_{\{1,0\}} - J^{(0,0,1)}_{\{1,0\}}\left(\xi_z\right)^{(1,0,0)}_{\{1,0\}}\right) \\
&\quad + B^2\left(2J^{(1,0,0)}_{\{1,-1\}}\left(\xi_z\right)^{(0,0,1)}_{\{1,1\}} + 2J_{\{1,-1\}}\left(\xi_z\right)^{(1,0,1)}_{\{1,1\}} - J^{(0,0,1)}_{\{1,-1\}}\left(\xi_z\right)^{(1,0,0)}_{\{1,1\}}\right) \\
&\quad + B^2\left(\left(\xi_x\right)^{(0,0,2)}_{\{1,0\}}\left(\xi_x\right)^{(1,0,0)}_{\{1,0\}} - \left(\xi_x\right)^{(0,0,1)}_{\{1,0\}}\left(\xi_x\right)^{(1,0,1)}_{\{1,0\}}\right) \\
&\quad + B^2\left(\left(\xi_z\right)^{(0,0,2)}_{\{1,0\}}\left(\xi_z\right)^{(1,0,0)}_{\{1,0\}} - \left(\xi_z\right)^{(0,0,1)}_{\{1,0\}}\left(\xi_z\right)^{(1,0,1)}_{\{1,0\}}\right) \\
&\quad + \rho g\left(J_{\{1,0\}}\left(\xi_x\right)^{(1,0,0)}_{\{1,0\}} + J_{\{1,-1\}}\left(\xi_x\right)^{(1,0,0)}_{\{1,1\}}\right)
\end{aligned} \tag{29}$$

$$\begin{aligned}
F_{x\{2,j\}} &= \left[\rho g + (B^2)' + \gamma p'\right]J_{\{2,j\}} - (B^2)'\xi^{(0,0,1)}_{z\{2,j\}} + B^2\xi^{(0,0,2)}_{x\{2,j\}} \\
&\quad + (B^2+\gamma p)J^{(1,0,0)}_{\{2,j+1\}} - \rho g\xi^{(1,0,0)}_{x\{2,j+1\}} - B^2\xi^{(1,0,1)}_{z\{2,j+1\}} \\
&\quad - \left[2\rho g + 3(B^2)' + \gamma(\gamma+1)p'\right]\frac{1}{2}\sum_{j_1=-1}^{j+1}J_{\{1,j_1\}}J_{\{1,j-j_1\}} \\
&\quad - \left[3B^2+\gamma(\gamma+1)p\right]\sum_{j_1=-1}^{j+2}J_{\{1,j_1\}}J^{(1,0,0)}_{\{1,j+1-j_1\}}
\end{aligned}$$

$$
\begin{aligned}
&+2(B^2)' \sum_{j_1=-1}^{j} J_{\{1,j_1\}} \left(\xi_z\right)^{(0,0,1)}_{\{1,j-j_1\}} \\
&-\frac{(B^2)'}{2} \sum_{j_1=0}^{j} \left(\left(\xi_x\right)^{(0,0,1)}_{\{1,j_1\}} \left(\xi_x\right)^{(0,0,1)}_{\{1,j-j_1\}} + \left(\xi_z\right)^{(0,0,1)}_{\{1,j_1\}} \left(\xi_z\right)^{(0,0,1)}_{\{1,j-j_1\}} \right) \\
&-B^2 \sum_{j_1=-1}^{j} \left(2J_{\{1,j_1\}} \left(\xi_x\right)^{(0,0,2)}_{\{1,j-j_1\}} + J^{(0,0,1)}_{\{1,j_1\}} \left(\xi_x\right)^{(0,0,1)}_{\{1,j-j_1\}} \right) \\
&+2B^2 \sum_{j_1=-1}^{j+1} \left(J^{(1,0,0)}_{\{1,j_1\}} \left(\xi_z\right)^{(0,0,1)}_{\{1,j+1-j_1\}} + J_{\{1,j_1\}} \left(\xi_z\right)^{(1,0,1)}_{\{1,j+1-j_1\}} \right) \\
&-B^2 \sum_{j_1=-1}^{j+1} J^{(0,0,1)}_{\{1,j_1\}} \left(\xi_z\right)^{(1,0,0)}_{\{1,j+1-j_1\}} \\
&+B^2 \sum_{j_1=0}^{j+1} \left(\left(\xi_x\right)^{(1,0,0)}_{\{1,j_1\}} \left(\xi_x\right)^{(0,0,2)}_{\{1,j+1-j_1\}} + \left(\xi_z\right)^{(1,0,0)}_{\{1,j_1\}} \left(\xi_z\right)^{(0,0,2)}_{\{1,j+1-j_1\}} \right) \\
&-B^2 \sum_{j_1=0}^{j+1} \left(\left(\xi_x\right)^{(1,0,1)}_{\{1,j_1\}} \left(\xi_x\right)^{(0,0,1)}_{\{1,j+1-j_1\}} + \left(\xi_z\right)^{(1,0,1)}_{\{1,j_1\}} \left(\xi_z\right)^{(0,0,1)}_{\{1,j+1-j_1\}} \right) \\
&+B^2 \sum_{\substack{j_1=0 \\ j\geq 1}}^{j-1} \left(\left(\xi_y\right)^{(1,0,0)}_{\{1,j_1\}} \left(\xi_y\right)^{(0,0,2)}_{\{1,j-1-j_1\}} - \left(\xi_y\right)^{(1,0,1)}_{\{1,j_1\}} \left(\xi_y\right)^{(0,0,1)}_{\{1,j-1-j_1\}} \right) \\
&+\rho g \sum_{j_1=-1}^{j+1} J_{\{1,j_1\}} \left(\xi_x\right)^{(1,0,0)}_{\{1,j+1-j_1\}}, \qquad j=0,1,2,\cdots
\end{aligned} \tag{30}
$$

$$\vdots$$

$$
\begin{aligned}
F_{y\{2,-4\}} &= (B^2+\gamma p) J^{(0,1,0)}_{\{2,-2\}} \\
&\quad - \left[3B^2+\gamma(\gamma+1)p\right] J_{\{1,-1\}} J^{(0,1,0)}_{\{1,-1\}}
\end{aligned} \tag{31}
$$

$$
\begin{aligned}
F_{y\{2,-3\}} &= (B^2+\gamma p) J^{(0,1,0)}_{\{2,-1\}} \\
&\quad - \left[3B^2+\gamma(\gamma+1)p\right] \left(J_{\{1,-1\}} J^{(0,1,0)}_{\{1,0\}} + J_{\{1,0\}} J^{(0,1,0)}_{\{1,-1\}} \right) \\
&\quad + B^2 \left(2J^{(0,1,0)}_{\{1,-1\}} \left(\xi_z\right)^{(0,0,1)}_{\{1,0\}} + 2J_{\{1,-1\}} \left(\xi_z\right)^{(0,1,1)}_{\{1,0\}} - J^{(0,0,1)}_{\{1,-1\}} \left(\xi_z\right)^{(0,1,0)}_{\{1,0\}} \right) \\
&\quad + \rho g J_{\{1,-1\}} \left(\xi_x\right)^{(0,1,0)}_{\{1,0\}}
\end{aligned} \tag{32}
$$

$$
\begin{aligned}
F_{y\{2,j\}} &= B^2 \xi^{(0,0,2)}_{y\{2,\substack{j-1 \\ j\geq 1}\}} + (B^2+\gamma p) J^{(0,1,0)}_{\{2,j+2\}} - \rho g \xi^{(0,1,0)}_{x\{2,j+2\}} - B^2 \xi^{(0,1,1)}_{z\{2,j+2\}} \\
&\quad - \left[3B^2+\gamma(\gamma+1)p\right] \sum_{j_1=-1}^{j+3} J_{\{1,j_1\}} J^{(0,1,0)}_{\{1,j+2-j_1\}} \\
&\quad + 2B^2 \sum_{j_1=-1}^{j+2} \left(J^{(0,1,0)}_{\{1,j_1\}} \left(\xi_z\right)^{(0,0,1)}_{\{1,j+2-j_1\}} + J_{\{1,j_1\}} \left(\xi_z\right)^{(0,1,1)}_{\{1,j+2-j_1\}} \right) \\
&\quad - B^2 \sum_{j_1=-1}^{j+2} J^{(0,0,1)}_{\{1,j_1\}} \left(\xi_z\right)^{(0,1,0)}_{\{1,j+2-j_1\}}
\end{aligned}
$$

$$
\begin{aligned}
&+B^2\sum_{j_1=0}^{j+2}\left((\xi_x)^{(0,1,0)}_{\{1,j_1\}}(\xi_x)^{(0,0,2)}_{\{1,j+2-j_1\}}-(\xi_x)^{(0,1,1)}_{\{1,j_1\}}(\xi_x)^{(0,0,1)}_{\{1,j+2-j_1\}}\right)\\
&+B^2\sum_{j_1=0}^{j+2}\left((\xi_z)^{(0,1,0)}_{\{1,j_1\}}(\xi_z)^{(0,0,2)}_{\{1,j+2-j_1\}}-(\xi_z)^{(0,1,1)}_{\{1,j_1\}}(\xi_x)^{(0,0,1)}_{\{1,j+2-j_1\}}\right)\\
&-B^2\sum_{\substack{j_1=-1\\ j\geq 1}}^{j-1}\left(2J_{\{1,j_1\}}(\xi_y)^{(0,0,2)}_{\{1,j-1-j_1\}}+J^{(0,0,1)}_{\{1,j_1\}}(\xi_y)^{(0,0,1)}_{\{1,j-1-j_1\}}\right)\\
&+B^2\sum_{j_1=0}^{j}\left((\xi_y)^{(0,1,0)}_{\{1,j_1\}}(\xi_y)^{(0,0,2)}_{\{1,j-j_1\}}-(\xi_y)^{(0,1,1)}_{\{1,j_1\}}(\xi_y)^{(0,0,1)}_{\{1,j-j_1\}}\right)\\
&+\rho g\sum_{j_1=-1}^{j+2}J_{\{1,j_1\}}(\xi_x)^{(0,1,0)}_{\{1,j+2-j_1\}},\qquad j=-2,-1,0,\cdots
\end{aligned}
\tag{33}
$$

$$
\begin{aligned}
F_{z\{2,-2\}} &= \gamma p J^{(0,0,1)}_{\{2,-2\}}\\
&\quad -\gamma(\gamma+1)pJ_{\{1,-1\}}J^{(0,0,1)}_{\{1,-1\}}
\end{aligned}
\tag{34}
$$

$$
\begin{aligned}
F_{z\{2,-1\}} &= \gamma p J^{(0,0,1)}_{\{2,-1\}}\\
&\quad -\gamma(\gamma+1)p\left(J_{\{1,-1\}}J^{(0,0,1)}_{\{1,0\}}+J_{\{1,0\}}J^{(0,0,1)}_{\{1,-1\}}\right)\\
&\quad +\rho g J_{\{1,-1\}}\xi^{(0,0,1)}_{x\{1,0\}}
\end{aligned}
\tag{35}
$$

$$
\begin{aligned}
F_{z\{2,j\}} &= \gamma p J^{(0,0,1)}_{\{2,j\}}-\rho g\xi^{(0,0,1)}_{x\{2,j\}}\\
&\quad -\gamma(\gamma+1)p\sum_{j_1=-1}^{j+1}J_{\{1,j_1\}}J^{(0,0,1)}_{\{1,j-j_1\}}\\
&\quad +\rho g\sum_{j_1=-1}^{j}J_{\{1,j_1\}}\xi^{(0,0,1)}_{x\{1,j-j_1\}},\qquad j=0,1,2,\cdots
\end{aligned}
\tag{36}
$$

$$\vdots$$

$$
J_{\{2,-2\}} = \xi^{(1,0,0)}_{x\{1,0\}}\xi^{(0,1,0)}_{y\{1,0\}}-\xi^{(0,1,0)}_{x\{1,0\}}\xi^{(1,0,0)}_{y\{1,0\}}
\tag{37}
$$

$$
\begin{aligned}
J_{\{2,-1\}} &= \xi^{(1,0,0)}_{x\{2,0\}}+\xi^{(0,1,0)}_{y\{2,0\}}\\
&\quad +\xi^{(1,0,0)}_{x\{1,0\}}\xi^{(0,1,0)}_{y\{1,1\}}+\xi^{(1,0,0)}_{x\{1,1\}}\xi^{(0,1,0)}_{y\{1,0\}}-\xi^{(0,1,0)}_{x\{1,0\}}\xi^{(1,0,0)}_{y\{1,1\}}-\xi^{(0,1,0)}_{x\{1,1\}}\xi^{(1,0,0)}_{y\{1,0\}}\\
&\quad +\xi^{(0,1,0)}_{y\{1,0\}}\xi^{(0,0,1)}_{z\{1,0\}}-\xi^{(0,0,1)}_{y\{1,0\}}\xi^{(0,1,0)}_{z\{1,0\}}+\xi^{(0,0,1)}_{z\{1,0\}}\xi^{(1,0,0)}_{x\{1,0\}}-\xi^{(1,0,0)}_{z\{1,0\}}\xi^{(0,0,1)}_{x\{1,0\}}
\end{aligned}
\tag{38}
$$

$$
\begin{aligned}
J_{\{2,j\}} &= \xi^{(0,0,1)}_{z\{2,j\}}+\xi^{(1,0,0)}_{x\{2,j+1\}}+\xi^{(0,1,0)}_{y\{2,j+1\}}\\
&\quad +\sum_{j_1=0}^{j+2}\left(\xi^{(1,0,0)}_{x\{1,j_1\}}\xi^{(0,1,0)}_{y\{1,j+2-j_1\}}-\xi^{(0,1,0)}_{x\{1,j_1\}}\xi^{(1,0,0)}_{y\{1,j+2-j_1\}}\right)\\
&\quad +\sum_{j_1=0}^{j+1}\left(\xi^{(0,1,0)}_{y\{1,j_1\}}\xi^{(0,0,1)}_{z\{1,j+1-j_1\}}-\xi^{(0,0,1)}_{y\{1,j_1\}}\xi^{(0,1,0)}_{z\{1,j+1-j_1\}}\right)
\end{aligned}
$$

$$+\sum_{j_1=0}^{j+1}\left(\xi^{(0,0,1)}_{z\{1,j_1\}}\xi^{(1,0,0)}_{x\{1,j+1-j_1\}}-\xi^{(1,0,0)}_{z\{1,j_1\}}\xi^{(0,0,1)}_{x\{1,j+1-j_1\}}\right),\quad j=0,1,2,\cdots \tag{39}$$

A. $\epsilon = n^{-1}$: Cowley-Artun (CA) Regime

As the mode grows, its magnitude ϵ can be measured by the ballooning scale $n^{-\frac{j}{2}}$ in the decreasing sequence of $j=\infty,\cdots,3,2,1,\cdots$. When the mode acquires the absolute order of $\epsilon = n^{-1}$, it enters a regime that was first modeled by Cowley and Artun [12]. In that regime, the mode is mostly incompressible, since at the lowest and dominant order, the plasma displacement is divergence-free

$$J_{\{1,-1\}} = \partial_x \xi_{x\{1,0\}} + \partial_y \xi_{y\{1,0\}} = 0 \tag{40}$$

The local eigenvalue equation for $\xi_{x\{1,0\}}$ remains the same as in the linear case, so that

$$\xi_{x\{1,0\}} = \xi_{x(1)}(x,y,\tau)H(z). \quad (\tau = n^{-\frac{1}{2}}t) \tag{41}$$

The dominant nonlinear term is the first order Jacobian $J_{\{2,-2\}}$, and nonlinear effects modify the envelope equation [12]

$$\frac{C_0}{\Gamma_{\rm A}^2}\partial_y^2\partial_\tau^2\xi_{x(1)} = C_1\frac{\Gamma^2}{\Gamma_{\rm A}^2}\partial_y^2\xi_{x(1)} + C_2\partial_x^2\xi_{x(1)} + C_3\partial_x^2\overline{\xi^2_{x(1)}}\partial_y^2\xi_{x(1)} + C_4\partial_y^2\xi^2_{x(1)} \tag{42}$$

where $\bar{A} \equiv L_y^{-1}\int_0^{L_y} dyA$ is the average over domain $0 < y < L_y$. The coefficients C_i $(i=0,\cdots,4)$ are determined by the equilibrium configuration and linear mode structure along field lines. The Cowley-Artun regime as governed by Eq. (42) is characterized by two orderings: $\Gamma^2/\Gamma_{\rm A}^2 \sim \mathcal{O}(n^{-1})$, and $\epsilon = n^{-1}$ (see Table I). The former ordering is a measure of the distance of the equilibrium away from marginal stability. The latter ordering applies when convection is small relative to the mode spatial scales, i.e. $\boldsymbol{\xi}\cdot\nabla \sim n^{-\frac{1}{2}} \ll 1$. Model equation (42) has a finite-time singular solution when the nonlinear term $C_4\partial_y^2\xi^2_{x(1)}$ becomes dominant. That is the so-called detonation mechanism first envisioned by Cowley and Artun [12]. The detonation regime where the C_4 nonlinear term dominates and the finite-time singular solution exists may be specified as follows:

$$\frac{C_1\Gamma^2}{C_4\Gamma_{\rm A}^2} \ll \xi_{x(1)} \sim \mathcal{O}(n^{-1})L_{\rm eq} \tag{43}$$

It is noted that the detonation regime is a rather narrow subset of the general Cowley-Artun regime where Eq. (42) applies. The equilibrium has to be sufficiently close to linear marginal

stability in order for the detonation regime to exist at all. Even within the detonation regime, the solution $\xi_{x(1)}$ may not demonstrate any finite-time singular behavior due to the small upper bound $\mathcal{O}(n^{-1})L_{\rm eq}$ for that regime.

	$\Gamma^2/\Gamma_{\rm A}^2 \sim \mathcal{O}(n^{-1})$	$\Gamma^2/\Gamma_{\rm A}^2 \sim \mathcal{O}(n^{-\frac{1}{2}})$	$\cdots$
$\epsilon = n^{-1}$	Cowley-Artun regime		
$\epsilon = n^{-\frac{1}{2}}$			
$\vdots$			

TABLE I: Nonlinear regimes of g-mode

B. $\epsilon = n^{-1/2}$: Beyond Cowley-Artun Regime

As the mode grows to larger magnitude at the order $\epsilon = n^{-1/2}$, the dominant nonlinear Jacobian scales as

$$J_{\{2,-2\}} \sim J_{\{1,-1\}} \sim \mathcal{O}(1)$$

so that the plasma compression of the dominant order, which is proportional to $J_{\{1,-1\}}$, is no longer zero. At this order of ϵ, nonlinear effects directly modify the local eigenvalue equation for $\xi_{x\{1,0\}}$. The Cowley-Artun model in Eq. (42) is not valid in this nonlinear regime. Direct MHD simulations of g-mode have been carried out recently in both a finite difference code (BIC) [16] and the code NIMROD [25]. In both cases, all MHD field components remains bounded in magnitude during the intermediate nonlinear phase. The growth rates are slightly lower than that of linear phase (Fig. 1). Simulation results also indicate plasma compression $\nabla \cdot \mathbf{u}$ remain small in linear to early nonlinear phase ($\epsilon = n^{-1}$); $\nabla \cdot \mathbf{u}$ starts to grow exponentially in intermediate nonlinear phase ($\epsilon = n^{-1/2}$) [16]. This results is consistent with our nonlinear analysis of the g-mode.

The absence of a distinctive Cowley-Artun regime ($\epsilon = n^{-1}$) in our direct MHD simulations may be due to its closeness to the intermediate regime where $\epsilon = n^{-\frac{1}{2}}$. For the typical mode number $n = 10$ used in simulations and observed in ELM experiments, $n^{-1} = 0.1$ and $n^{-\frac{1}{2}} \sim 0.3$ respectively. Mathematically, as $n \to \infty$ the two regimes should be more separated. However, the absolute magnitude of the mode in the CA regime will also be approaching zero as $n \to \infty$, a situation that is physically irrelevant. In addition, the

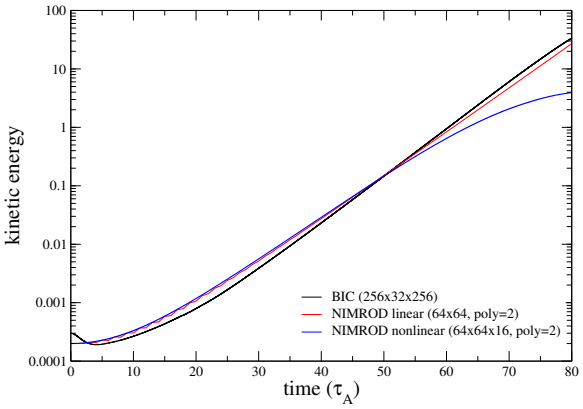

FIG. 1: Growth of kinetic energy of a g-mode in direct MHD simulations using the finite difference code BIC and code NIMROD [25].

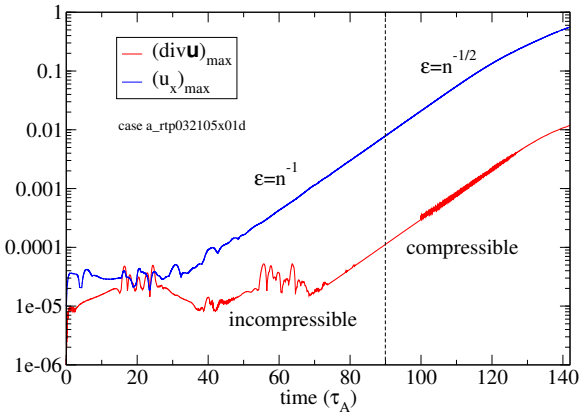

FIG. 2: Growth of the maximum x-component (blue line) and the maximum divergence (red line) of the velocity field of the line-tied g-mode in a direct MHD simulation [16].

asymptotic limit $n \to \infty$ is also where the ideal MHD model no longer applies. Nevertheless, it remains a numerical challenge to explore the nonlinear regimes of g-mode in the $n \to \infty$ limit in direct MHD simulations.

C. Governing Equations for Intermediate Nonlinear Regime

In order to derive the governing equations for the intermediate nonlinear regime of g-mode, we set $\epsilon = n^{-1/2}$ in expansion (3) so that

$$\boldsymbol{\xi}(\sqrt{n}x_0, ny_0, z_0, t) \;=\; n^{-\frac{1}{2}} \sum_{j=0}^{\infty} n^{-\frac{j}{2}} \left(\hat{x}\xi_{x(\frac{j}{2})} + \frac{\hat{y}}{\sqrt{n}}\xi_{y(\frac{j}{2})} + \hat{z}\xi_{z(\frac{j}{2})} \right) \tag{44}$$

$$J(\sqrt{n}x_0, ny_0, z_0, t) \;=\; 1 + \sum_{j=0}^{\infty} n^{-\frac{j}{2}} J_{\frac{j}{2}} \tag{45}$$

At the lowest order the three components of Eq. (1) are

$$\sqrt{n}\frac{B^2 + \gamma p(1+J_0)^{2-\gamma}}{(1+J_0)^3}\partial_x J_0 \;=\; 0, \tag{46}$$

$$n\frac{B^2 + \gamma p(1+J_0)^{2-\gamma}}{(1+J_0)^3}\partial_y J_0 \;=\; 0, \tag{47}$$

$$\gamma p(1+J_0)^{-1-\gamma}\partial_z J_0 \;=\; 0, \tag{48}$$

where $J_0 = \partial_x \xi_{x(0)} + \partial_y \xi_{y(0)} + [\xi_{x(0)}, \xi_{y(0)}]$, and $[A, B] \equiv \partial_x A \partial_y B - \partial_y A \partial_x B$. Together with $\int d\mathbf{r}_0 J = 1$ we have $J_0 = 0$. The lowest order plasma compression, which is proportional to $\partial_x \xi_{x(0)} + \partial_y \xi_{y(0)}$, is therefore nonzero in general due to nonlinearity. The next order expansion of Eq. (1) in $n^{-\frac{1}{2}}$ yields

$$(\gamma p + B^2) J_{\frac{1}{2}} - B^2 \partial_z \xi_{z(0)} - \rho g \xi_{x(0)} = F_1(z,t), \tag{49}$$

$$\rho \partial_t^2 \xi_{z(0)} = \gamma p \partial_z J_{\frac{1}{2}} - \rho g \partial_z \xi_{x(0)}, \tag{50}$$

where $F_1(z,t)$ is a function to be determined, and

$$\begin{aligned} J_{\frac{1}{2}} \;=\; & \partial_x \xi_{x(\frac{1}{2})} + \partial_y \xi_{y(\frac{1}{2})} + \partial_z \xi_{z(0)} \\ & + (\partial_y \xi_{y(0)} \partial_z \xi_{z(0)} - \partial_z \xi_{y(0)} \partial_y \xi_{z(0)}) + (\partial_z \xi_{z(0)} \partial_x \xi_{x(0)} - \partial_x \xi_{z(0)} \partial_z \xi_{x(0)}) \\ & + (\partial_x \xi_{x(0)} \partial_y \xi_{y(\frac{1}{2})} - \partial_y \xi_{x(0)} \partial_x \xi_{y(\frac{1}{2})}) + (\partial_x \xi_{x(\frac{1}{2})} \partial_y \xi_{y(0)} - \partial_y \xi_{x(\frac{1}{2})} \partial_x \xi_{y(0)}) \\ & + (\partial_z \xi_{y(0)} \partial_x \xi_{z(0)} - \partial_x \xi_{y(0)} \partial_z \xi_{z(0)}) \partial_y \xi_{x(0)} \\ & + (\partial_z \xi_{z(0)} \partial_x \xi_{x(0)} - \partial_x \xi_{z(0)} \partial_z \xi_{x(0)}) \partial_y \xi_{y(0)} \\ & + (\partial_z \xi_{x(0)} \partial_x \xi_{y(0)} - \partial_x \xi_{x(0)} \partial_z \xi_{y(0)}) \partial_y \xi_{z(0)}. \end{aligned} \tag{51}$$

At the third order the equation for $\xi_{x(0)}$ may be obtained by applying the operator $\hat{z} \cdot \nabla \times$ to Eq. (1). It follows that

$$\begin{aligned} & \rho \partial_y \partial_t^2 \xi_{x(0)} + \rho [\xi_{x(0)}, \partial_t^2 \xi_{x(0)}] \\ & = \; \partial_y \left\{ (\rho g + (B^2)' + \gamma p') J_{\frac{1}{2}} - (B^2)' \partial_z \xi_{z(0)} + B^2 \partial_z^2 \xi_{x(0)} \right\} \\ & \quad + \rho g [\xi_{x(0)}, J_{\frac{1}{2}}] + B^2 [\xi_{x(0)}, \partial_z^2 \xi_{x(0)}] \end{aligned} \tag{52}$$

From Eqs. (49), (51), and the no-slip, solid wall boundary condition at $x = 0, L_x$, it turns out that

$$F_1(z,t) = (\gamma p + B^2) \partial_x \xi_{x(\frac{1}{2})}|_{x=0,L_x}. \tag{53}$$

Since the mode is localized in the gradient region even in nonlinear phase, one may assume $\partial_x \xi_{x(\frac{1}{2})}|_{x=0,L_x} \sim 0$ at boundaries in x direction that is far away from the gradient region. This leads to closure condition $F_1(z,t) = 0$. In that case, Eqs. (51), (50), and (52) compose a closed model equation system governing the intermediate nonlinear phase of g-mode.

Denote the linear local ballooning equations for g-mode as

$$\partial_t^2 \xi_{x(0)} = \mathcal{L}_x(\xi_{x(0)}, \xi_{z(0)}), \tag{54}$$

$$\partial_t^2 \xi_{z(0)} = \mathcal{L}_z(\xi_{x(0)}, \xi_{z(0)}). \tag{55}$$

For the sake of comparison, tbe governing equations for $\epsilon = n^{-\frac{1}{2}}$ regime can be written in a more compact form

$$\begin{aligned} &\partial_y \left(\partial_t^2 \xi_{x(0)} - \mathcal{L}_x(\xi_{x(0)}, \xi_{z(0)})\right) + [\xi_{x(0)}, \partial_t^2 \xi_{x(0)}] \\ &\quad = \frac{gB^2}{\gamma p + B^2}[\xi_{x(0)}, \partial_z \xi_{z(0)}] + \frac{B^2}{\rho}[\xi_{x(0)}, \partial_z^2 \xi_{x(0)}], \end{aligned} \tag{56}$$

$$\partial_t^2 \xi_{z(0)} = \mathcal{L}_z(\xi_{x(0)}, \xi_{z(0)}). \tag{57}$$

Clearly, during this nonlinear phase, nonlinearity directly and only modifies the x component of local ballooning mode equations.

V. SUMMARY AND DISCUSSION

In summary, nonlinear g-mode evolves sequentially through $\epsilon = n^{-1}$, $\epsilon = n^{-1/2}$, ..., phases ($\epsilon \sim$ normalized mode amplitude, $n \sim k_\perp/k_\parallel$). For equilibriums that are close to linear marginal stability [$\Gamma^2/\Gamma_{\rm A}^2 \sim \mathcal{O}(n^{-1})$], the Cowley-Artun regime is recovered in the early nonlinear phase when $\epsilon = n^{-1}$. The detonation regime, as specified in (43), is a rather narrow subset of the general Cowley-Artun regime where Eq. (42) applies. Even within the detonation regime, the solution $\xi_{x(1)}$ may not demonstrate any finite-time singular behavior due to the small upper bound $\mathcal{O}(n^{-1})L_{\rm eq}$ for that regime. In the intermediate nonlinear phase when $\epsilon = n^{-1/2}$, the lowest order plasma compression [$\nabla \cdot \boldsymbol{\xi} \sim \mathcal{O}(1)$] is nonzero and the model equation in Eq. (42) for CA regime does not apply. In the intermediate nonlinear phase ($\epsilon = n^{-1/2}$), nonzero plasma compression may reduce nonlinear growth and deplete the explosive nonlinearity beyond the order $\epsilon = n^{-1}$. This scenario is supported by the result of direct MHD simulations of a line-tied g-mode, which covers both the CA regime in early nonlinear phase and the intermediate nonlinear phase beyond the CA regime. The essential

role of plasma compression is also suggested by the model equations we have derived for the intermediate nonlinear phase. We plan to analyze the model equations and compare with direct MHD simulations next.

Acknowledgments

This research is supported by U.S. Department of Energy under Grant No. DE-FG02-86ER53218. Computations were performed in National Energy Research Scientific Computing Center, which is supported by U.S. Department of Energy under Contract No. DE-AC03-76SF00098. The authors are grateful for discussions with A. Bhattacharjee, J. D. Callen, and S. C. Cowley.

---

[1] C. C. Hegna, J. W. Connor, R. J. Hastie, and H. R. Wilson, *Phys. Plasmas* **3**, 584 (1996).

[2] P. B. Snyder, H. R. Wilson, J. R. Ferron, L. L. Lao, A. W. Leonard, T. H. Osborne, A. D. Turnbull, D. Mossessian, M. Murakami, and X. Q. Xu, *Phys. Plasmas* **9**, 2037 (2002).

[3] A. Bhattacharjee, Z. W. Ma, and X. Wang, *Geophys. Rev. Lett.* **25**, 861 (1998).

[4] P. Zhu, A. Bhattacharjee, and Z. W. Ma, *Phys. Plasmas* **10**, 249 (2003).

[5] P. Zhu, A. Bhattacharjee, and Z. W. Ma, *J. Geophys. Res.* **109**, A11211 (2004).

[6] E. G. Zweibel and D. L. Bruhwiler, *Astrophys. J.* **399**, 318 (1992).

[7] B. H. Fong, O. A. Hurricane, and S. C. Cowley, *Solar Phys.* **201**, 93 (2001).

[8] Z. W. Ma and A. Bhattacharjee, *Geophys. Rev. Lett.* **25**, 3277 (1998).

[9] S. Zaharia and C. Z. Cheng, *Geophys. Rev. Lett.* **30**, 1883 (2003).

[10] G. A. Gary, *Solar Phys.* **203**, 71 (2001).

[11] I. O. Voronkov, E. F. Donovan, P. Dobias, V. I. Prosolin, M. Jankowska, and J. C. Samson, in *Proceedings of the 7th International Conference on Substorms (ICS-7), Levi, Finland, 2004* (2004), p. 140.

[12] S. C. Cowley and M. Artun, *Phys. Rep.* **283**, 185 (1997).

[13] O. A. Hurricane, B. H. Fong, S. C. Cowley, F. V. Coroniti, C. F. Kennel, and R. Pellat, *J. Geophys. Res.* **104**, 10,221 (1999).

[14] H. R. Wilson and S. C. Cowley, Phys. Rev. Lett. **92**, 175006 (2004).

[15] B. H. Fong, Ph.D. thesis, Princeton University (1999).

[16] P. Zhu, A. Bhattacharjee, and K. Germaschewski, Phys. Rev. Lett. **Accepted** (2005).

[17] W. Park, E. D. Fredrickson, A. Janos, J. Manickam, and W. M. Tang, Phys. Rev. Lett. **75**, 1763 (1995).

[18] H. Lutjens and J.-F. Luciani, *Phys. Plasmas* **4**, 4192 (1997).

[19] Y. Nishimura, J. D. Callen, and C. C. Hegna, *Phys. Plasmas* **6**, 4685 (1999).

[20] R. Kleva and P. N. Guzdar, *Phys. Plasmas* **8**, 103 (2001).

[21] D. Pfirsch and R. N. Sudan, *Phys. Fluids B* **5**, 2052 (1993).

[22] R. L. Dewar and A. H. Glasser, *Phys. Fluids* **26**, 3038 (1983).

[23] E. Hameiri, *Phys. Plasmas* **6**, 674 (1999).

[24] J. W. Connor, R. J. Hastie, and J. B. Taylor, Proc. R. Soc. Lond. A. **365**, 1 (1979).

[25] P. Zhu, C. C. Hegna, and C. R. Sovinec, in *47th Annual Meeting of the Division of Plasma Physics, American Physical Society, 24-28 October 2005, Denver, CO* (American Physical Society, 2005), poster LP1.00059.